Progressive damage analysis and optimization of winding angle and geometry for a composite pressure hull wound using geodesic and planar patterns

Amir Molavizadeh[1] **, Abdolmajid Rezaei**[1]

Abstract Recently, it has been found that submarine pressure hulls constructed from fiber-reinforced multilayers have great potential to replace classical metallic ring-stiffened pressure hulls. The strength and stability of these structures are the most important functional requirements and should be considered in any design procedure. This study aimed to optimize the strength and buckling stability of elliptical composite deep-submerged pressure hulls using two different filament winding patterns, namely geodesic and planar. The numerical modeling of the pressure hull under hydrostatic was carried out using the Finite Element Method (FEM) in ABAQUS using Python script and a damage model written as a User MATerial (UMAT) Subroutine. Puck failure criterion was chosen for failure prediction. The results suggest that both buckling and static material failure should be considered in the design of a composite pressure hull. Moreover, it was shown that the optimum pressure hull has a geodesic filament winding pattern with a/b (the ratio between two diameters) =1.2 and the winding angle of 45°. Based on the progressive failure criterion, for such an optimum design, failure initiates at an applied load of 28.6 MPa and the pressure hull withstands to 40.3 MPa.

Keywords: Composite pressure hull; Geodesic winding; Planar winding; Puck failure criterion; Python; UMAT

1. Introduction

Composite submersible pressure hulls have significant advantages over metallic pressure hulls due to their high stiffness to weight ratio, low density, corrosion resistance, and improved formability [1]. Ideally, a pressure hull structure should have the minimum weight for a given applied pressure. The hull density also must be adjusted as near as possible to the density of sea water. Using these structural materials leads to a considerable reduction in operations and costs [2]. Composites also have considerable potential stealth bonus [4] as there is scope for incorporating damping, decoupling and anechoic characteristics to improve the acoustic stealth [2].

Among all composite manufacturing processes, filament winding (FW) stands out due to high precision in fiber positioning, high fiber content, good automation capability, and low void content. These advantageous of filament winding make it the most common process for manufacturing revolution and axisymmetric parts, such as pressure vessels [5]. Under excessive uniaxial or biaxial compression loading, the shell structure initially starts to deform uniformly, a point is reached at which increasing compression load yields buckling. Correspondingly, the composite under loading may fail due to global or local buckling. Typically, such a failure is occurred in two distinct ways: the propagation of radial displacements followed by global buckling resulting in collapse, or just a sudden collapse. It should be noted here that load prediction is much more difficult for composite structures than for metallic materials [7]. For instance, in the case where the composite is too thick, it is possible that buckling does not occur and the structure fails due to material failure [8].

Many researches have been performed on buckling phenomenon, post buckling, and fracture of composite structures by experiment and finite element method. Hojati [9] found that geodesic and semi geodesic winding methods have some limitations. He suggested new method based on geodesic path and classical laminated theory. The results he obtained indicated that resin has an important role in the design of composite pressure hull domes.

Blachet[10] studied buckling and failure based on Tsai-Hill criterion for a composite spherical shell. He also considered effect of radius to thickness ratio, boundary condition and winding angle on buckling behavior of composite spherical shell. Mian et al.[11] presented the optimization procedure for composite pressure vessel design considering both Tsai-Wu failure and the maximum stress criteria for first-ply failure. The optimization results showed that for all of studied composite material systems the angle-ply

✉ Amir Molavizadeh

a.molavizadeh@alumni.iut.ac.ir

[1] Mechanical Department, Isfahan University of Technology (IUT), Isfahan, 84156-83111, Iran

[±θ] was the optimum lay-up. Walker [12] described a technique for combining genetic algorithms (GA) and the finite element method to minimize both the mass and deflection using a multi-objective approach.

Rao et al. [13] tried to predict the minimum buckling load with and without stiffener for the composite shell of continuous angle ply laminae. Jacob et al. [14] presented a methodology for the multi-objective optimization of laminated composite materials. The fiber orientations and fiber volume fractions of the lamina were considered as the variables for optimization. Herbert et al. [15] studied the structural optimization of laminated composite materials using the genetic algorithm and neural networks. Marín et al. [16] developed an optimization procedure for the geometric design of a composite material stiffened panel. Topal [17] carried out a multi-objective design for symmetrically angle-ply laminated plates under biaxial compressive buckling and uniform thermal loads. Lee [18] optimized composite sandwich cylinders under external hydrostatic pressure and concluded that with increasing the thickness of sandwich a point is reached where buckling load exceeds the critical failure load of material. Therefore, the optimum point is determined based on material failure. Based on these results, Lee [18] proposed that both buckling and static material failure should be considered in the design of composite sandwich cylinder. Moreover, Kaustav [19] studied the first-ply failure of thin composite conidial shells subjected to uniformly distributed load to achieve higher failure value.

Liang et [21] introduced an optimized design of filament-wound multilayer sandwich submersible pressure hulls and showed that facings become thicker and cores become thinner as operational depth increases. Zu et al [22], with an aim to maximize the structural performance of pressure vessels, presented an optimal design of a half-cell dome profile for filament wound articulated pressure vessels based on Tsai-Wu failure criterion. Tanguy et al. [24] studied the optimal design of deep submarine exploration housings and autonomous underwater vehicles. The structures investigated by Tanguy et al. [24] were thin-walled laminated composite unstiffened vessels. Structural buckling failure due to high external hydrostatic pressure was the dominant risk factor at exploitation conditions. They also investigated the fiber orientations of composite cylinders that maximize the stability limits. A genetic algorithm procedure coupled with an analytical model of shell buckling was developed to determine numerically optimized stacking sequences. Karam and Maalawi [25] developed a practical approach for enhancing the buckling stability of thin-walled anisotropic rings/long cylinders.

Almeida [26] investigated the failure of carbon fiber reinforced epoxy filament wound composite tubes subjected to hydrostatic external pressure using experiment and numerical analyses. He also used finite element analysis through the arc length method along with progressive failure analysis based on a proposed damage model was to predict external pressure. The failure pressures were also estimated in [26].

Humberto [27], with an aim to predict the failure of carbon fiber/epoxy filament wound composite tubes under radial compressive loading, focused on the development of a computational model with damage. Numerical analysis was performed using finite element method (FEM) accompanied with a damage model written as a UMAT and linked to ABAQUS. Both numerical and experimental results led to the conclusion that the predominant failure mode was delamination.

There are few studies concerning the composite pressure hulls constructed by a filament winding method. In all methods of winding, parameters such as winding angle and the shape of dome area affect structure considerably. In the present study, in order to obtain an optimum composite pressure hull, these two parameters are optimized. It is worth noting that obtaining an optimized vessel necessitates considering buckling pressure criterion and failure criterion simultaneously. Moreover, in the simulation of filament wound composite pressure hull, considering the angle distribution and suitable sequence layup, especially in dome area, is of great importance. In the simulations presented here, in order to obtain precise results, Python codes have been employed. This is due to the fact that this method is able to model variations in thickness and winding angle of dome in a smooth manner. It is obvious that choosing an appropriate criterion is essential in detecting initial and progressive failure of composite pressure hulls applied pressure. In addition, a failure criterion which has the best agreement with experimental data is proposed. Moreover, a UMAT subroutine is written to identify failure initiation and model progressive failure.

2. Winding equations

The first step in the designing a filament wound structure consists of designing a mandrel and the calculation of the fiber path. Slippage of fiber winding on the surface of mandrel is one of the most important issues that must be addressed in this step.

The slippage tendency (λ) is defined as the ratio of oblique force to normal force and can be written as Eq. (1):

$$\lambda = \left|\frac{\overrightarrow{f_b}}{\overrightarrow{f_n}}\right| \leq |\mu| \tag{1}$$

where $\bar{f}$ is fiber tension vector, $\overrightarrow{f_r}$ is the force vector towards the center of curvature, $\overrightarrow{f_n}$ and $\overrightarrow{f_b}$ are the normal force and tangential oblique force applied to the surface of the mandrel, respectively and μ is the friction factor between fiber and mandrel which depends strongly on resin viscosity and varies from 0.2 (wet winding) to 0.39 (dry winding). The geometry of fibers path on the surface of mandrel is shown in Fig. 1.

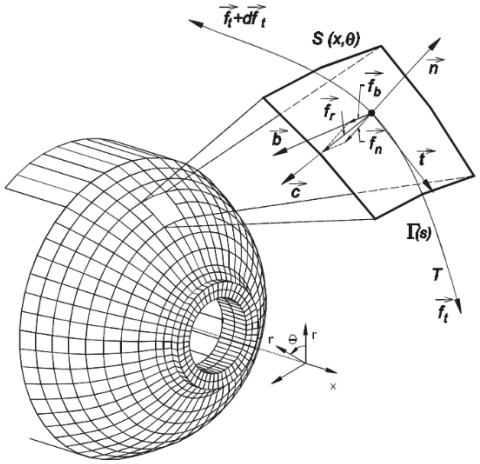

Fig. 1 Geometry of fibers path on the surface [28]

By considering tangential and perpendicular forces applied on the surface and substituting them in Eq. (1), λ can be expressed as [24]:

$$\lambda = \frac{A^2 r' sin\alpha + A^3 r \frac{d\alpha}{d\xi}}{A^3 sin^2\alpha - r r'' cos^2\alpha} \tag{2}$$

where ξ is the variable of fiber path, r' and r'' are the first and second differential of radial coordinate with respect to x-coordinate, respectively and A equals $\sqrt{1 + r'^2}$.

On a given a mandrel's surface , fibers tend to follow the geodesic path, which is, the shortest distance between two points on a surface . In geodesic winding, winding angle is calculated by setting λ to zero in Eq. (2). In Eq. (3) which is known as Clairaut's equation, α_0 and R are winding angle and radius of the vessel in the cylindrical segment, respectively (see Fig. 2).

$$sin\alpha_n = \frac{R}{\rho_n} sin\alpha_c \tag{3}$$

where R, ρ_n, α_c and α_n are cylinder radius, radius in the dome, winding angle in the cylindrical segment and angle winding in dome, respectively. Moreover , ρ_n varies between the opening radius and R and α_n varies between α_c and 90^0.

When the pressure hull is wrapped, resins are accumulated at the entrance due to the dome geometry. Considering a constant number of fibers in all sections, the wound composite thickness distribution along the composite dome can be written as follows:

$$t_n = \frac{R}{\rho_n} \frac{\cos(\alpha_0)}{\cos(\alpha_n)} t_0 \tag{4}$$

where t_n and t_0 are the thicknesses of the helical layers on the dome and cylinder, respectively.

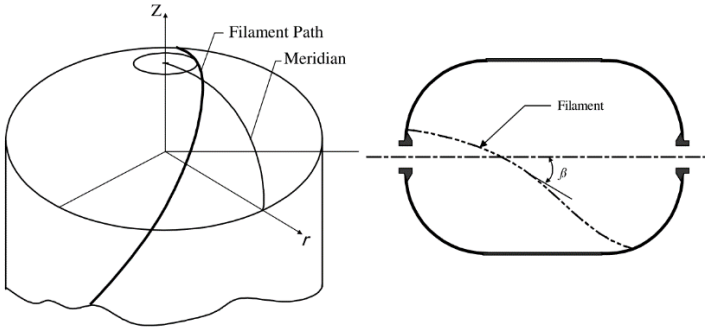

Fig. 2 Schematic of geodesic winding path [29]

One of the difficulties enc for winding machines. Obviously, such a treatment ot be used, mostly due to the fact that the geometry s an appropriate choice in such cases. Using this metl ic representation of the winding method is given in Fig. **3**. The angle of winding may be calculated as:

$$\alpha = \tan^{-1}\left(\frac{R_1+R_2}{L}\right) \tag{5}$$

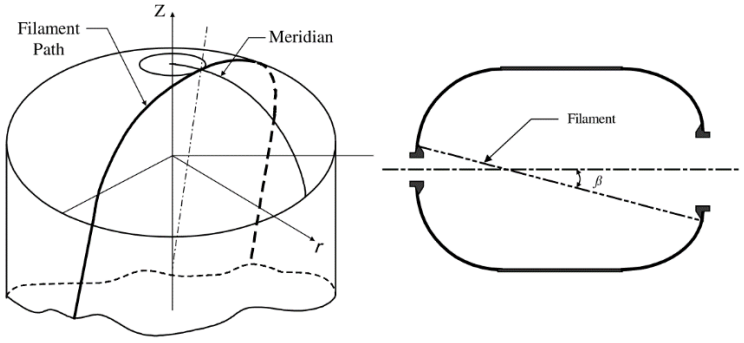

Fig. 3 Schematic of planar winding segment [29]

where R_1 and R_2 are radii of openings and L indicates the length of pressure vessel.

In polar coordinate system, fiber position on the dome region is presented by x_0, r and θ that are longitudinal, radial and angular positions, respectively. Obtaining the derivatives with respect to these variables are important to determine α and the tendency towards slippage. Radius of bandwidth middle line (r_p), depth of dome (d), band width (BW), opening radius (r_o), angle of the line perpendicular to geometry (φ_{cone}), and height (h_{cone}) are the remaining parameters. The section area of the cylindrical segment of composite region is given by Eq. (6) [30]:

$$A_{cyl} = \pi[(r_{cyl} + t_{cyl})^2 - r_{cyl}{}^2] \tag{6}$$

and Eq. (7) is used to calculate the wound composite thickness on the dome area

$$t = \frac{-2\pi r + \sqrt{4\pi^2 r^2 + 4\pi \sin(\varphi) A_{cyl}\left(\frac{\cos\alpha_c}{\cos\alpha}\right)}}{2\pi \sin(\varphi)} \tag{7}$$

ırface excluding the band that is adjacent to opening [30]. n this region by considering the area as a planar ring (see Fig. **4**). Based on this approach, the thickness can be calculated as follows:

$$t_{avg} = \frac{V}{\pi[(r_0 + BW)^2 - r_o{}^2]} \tag{8}$$

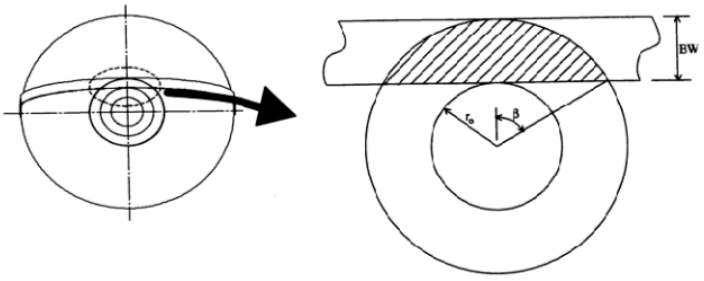

Fig. 4 Schematic of the opening adjacent band in planar winding [30]

3. Failure theories

Soden et al. [31] studied the different failure criteria for failures occurring in composites. They compared existing failure criteria in "The World Wide Failure Exercise (WWFE)" for different specimens with different boundary conditions and different loadings modes. According to their study, the Puck failure criterion shows the best agreement with experimental in comparison with other criteria. This is why this criterion was employed in this study.

3.1 Puck failure Criterion

Puckbelieves that the failure in fiber and matrix should be investigated separately.

Considering the linear elastic behavior of the material and the constraint between fiber and matrix, composite strain in the direction along fiber is the same as that in the fiber strain. Therefore, the tensile (X_{fT}) and compressive (X_{fT}) strengths of fiber can be calculated using Eq.(9) [33].

$$X_{fT} = \varepsilon_{f1}E_{f1} = \frac{X_T}{E_1}E_{f1} = \varepsilon_{1T}E_{f1}$$
$$X_{fC} = \varepsilon_{f1}E_{f1} = \frac{X_C}{E_1}E_{f1} = \varepsilon_{1C}E_{f1} \quad (9)$$

where ε_{1T}, ε_{1C}, and $\varepsilon_{f1}$are the composite failure strain under tension and compression and the fiber failure strain, respectively. X_T and X_C represent the tensile (X_{fT}) and compressive (X_{fT}) strengths of composite layer and E_{f1} is the fiber elastic modulus.

Due to the fact that the transverse Young's modulus is different in matrix and fiber, Puck criterion uses a modification of Hook's equation for strain calculation.

Experimental results indicate that as τ_{21} increases in compression mode ($\sigma_1 < 0$), the compressive strength along fiber direction decreases. Based on these observations, and using laboratory techniques, Puck modified Hook's equation by adding the term $(10\gamma_{12})^2$ and suggested the following equation:

$$\frac{1}{\varepsilon_{1T}}\left(\varepsilon_1 + \frac{\upsilon_{f12}}{E_{f1}}m_{\sigma f}\sigma_2\right) = 1 \text{ if } \sigma_1 \geq 0 \quad (10)$$

$$\frac{1}{\varepsilon_{1C}}\left(\varepsilon_1 + \frac{\upsilon_{f12}}{E_{f1}}m_{\sigma f}\sigma_2\right) + (10\gamma_{12})^2 = -1 \; if \; \sigma_1 < 0$$

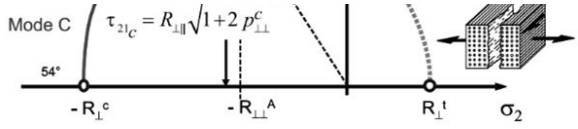

ithout any significant plastic deformation. Therefore, Puck conture experiments performed under transverse pressure loading, alue is usually slightly more than 45°. As it can be seen from

Fig. **5** , fracture angle varies between $\theta_{fp} = 0$ (Mode A) and $\theta_{fp} \neq 0$ (Mode B and Mode C).

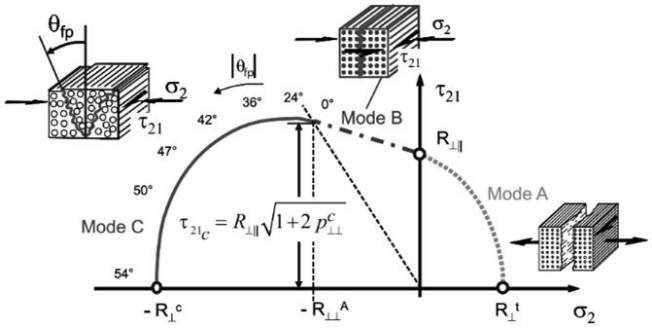

Fig. 5 Composite material Puck failure curve in the case of plane stress and $\boldsymbol{\sigma_1 = 0}$ for three different failure mode [34]

Afterwards, Puck incorporates the strength and material elastic properties separately using two degradation models.

Based on experiment weakening factor (f_w) can be expressed as follows:

$$f_w = 1 - \frac{\sigma_1}{\sigma_{1D}} = 1 - \left(\frac{\sigma_1}{\sigma_{1d}}\right)^n \tag{11}$$

where σ_{1d} is $1.1X_T$ and $-1.1X_C$ for tension and compression failure modes, respectively, and n is set 6 and 8 for matrices with high and low failure strain [33].

This reduced properties produces factor η multiplying by initial moduli (Eq.(12)). By introducing $f_{E(IFF)}$ in Eq. (13), Puck suggests that material reduction factor η can be calculated using Eq. (14) for $f_{E(IFF)} > 1$ in the case where failure occurs in matrix [33]:

$$\begin{pmatrix} E_\perp \\ G_{\perp\parallel} \end{pmatrix} = \begin{pmatrix} \eta_E E_{\perp s} \\ \eta_G G_{\perp\parallel s} \end{pmatrix} \tag{12}$$

$$f_{E(IFF)} = \sqrt{\left(\frac{\tau_{21}}{S_{21}}\right)^2 + \left(1 - p_{\perp\parallel}^{(+)} \frac{Y_T}{S_{21}}\right)^2 \left(\frac{\sigma_2}{Y_T}\right)^2} + p_{\perp\parallel}^{(+)} \frac{\sigma_2}{S_{21}} + \left|\frac{\sigma_1}{\sigma_{1D}}\right| \tag{13}$$

Inter fiber failure modes have different property reduction trends. In the modes A and C, the elastic moduli E_{22} and G_{12} are reduced, while in the mode B only modulus G_{12} is reduced. Knops [35] studied graphite and glass internal pressure vessel experimentally and reported the Puck property reduction curve under transverse tension (i.e. in cases where $\sigma_2 \geq 0$). According to Knops [35], this curve can be defined by Eq. (16). Parameters of the equation are given in Table 1. In the present study, two parameters, namely η_E and η_G were used

$$\eta_E = \frac{1 - \eta_{rE}}{1 + c_E\left(f_{E(IFF)} - 1\right)^{\xi_E}} + \eta_{rE}$$

$$\eta_G = \frac{1 - \eta_{rG}}{1 + c_G\left(f_{E(IFF)} - 1\right)^{\xi_G}} \tag{14}$$

Table 1 Proposed values in Knops reduction function for Glass and Carbon [35]

Parameter	CFRP		GFRP	
	$G_{\perp\parallel}$	$E_\perp$	$G_{\perp\parallel}$	$E_\perp$
c	0.95	5.3	0.7	5.3
ξ	1.17	1.3	1.5	1.3
η_r	0.67	0.03	0.25	0.03

4. Optimization of composite pressure hull

A composite pressure hull with a length of 2200 mm and a diameter of 1100 mm was considered for simulation. Moreover, the cone height was assumed to have a constant value of 20 mm in all the models. The simulation of composite pressure hull was performed in ABAQUS.

In this study, two approaches were employed to simulate composite pressure hull. During the first approach, the thickness and winding angle of each segment of vessel were calculated initially using MATLAB software. Afterwards, the thickness and winding angle were determined for each segment. There were considerable amount of discontinues near the vessel opening because of the extreme changes in the thickness and winding angle. During the second approach, scripting by Python language was employed to determine the angle, thickness and layup for each element in ABAQUS.

The line graph in 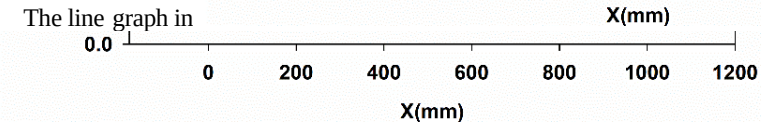

site pressure according to the results obtained from t can be seen from Fig. **6**, the variation of the failure criterion along the length of composite pressure hull is smoother in the scripting method in comparison with that in the partition method. This indicates that using scripting method leads to more reasonable results. It should also be noted that all steps of simulation in the scripting method including geometry modeling, material assigning, and considering boundary conditions executed autonomously. The flowchart of the method used for the optimization is shown in Fig. 7.

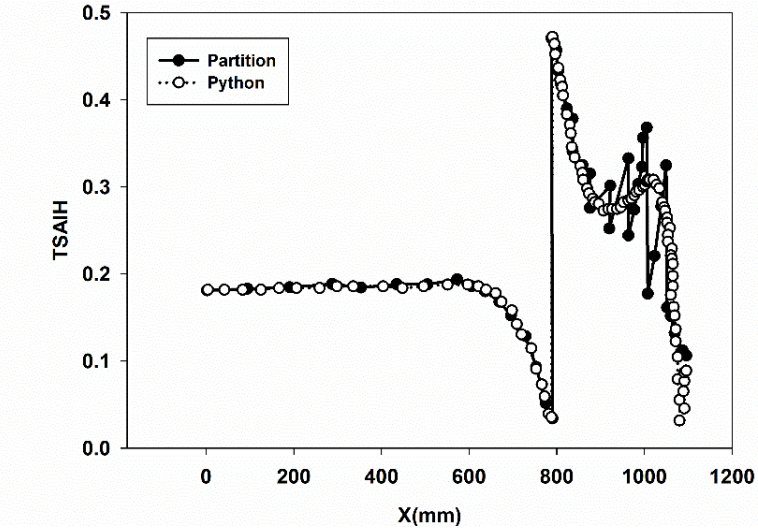

Fig. 6 Tsai-Hill failure criterion results of modeling with scripting and partition methods through length of vessel

Shell element (S4R) with reduced integration was used in this simulation. During all of the simulations, Tsai-Hill criterion is applied to detect failure. In the scripting method for static analysis, in order to reduce the number of elements and save the analysis time, one 360th part of a full circle (one degree) was modeled and the symmetry boundary conditions were applied (see Fig. 8). However, in the buckling analysis, composite pressure hull is modeled completely. In the following, filament wound geometry, material properties and the layup and the results obtained from the simulation of geodesic winding and planar winding are reported. Finally, the optimum composite pressure hull for each filament winding method are selected. As is usual, first Eigen value (no rigid motion) for buckling analysis is considered since it is more important than the other Eigen values.

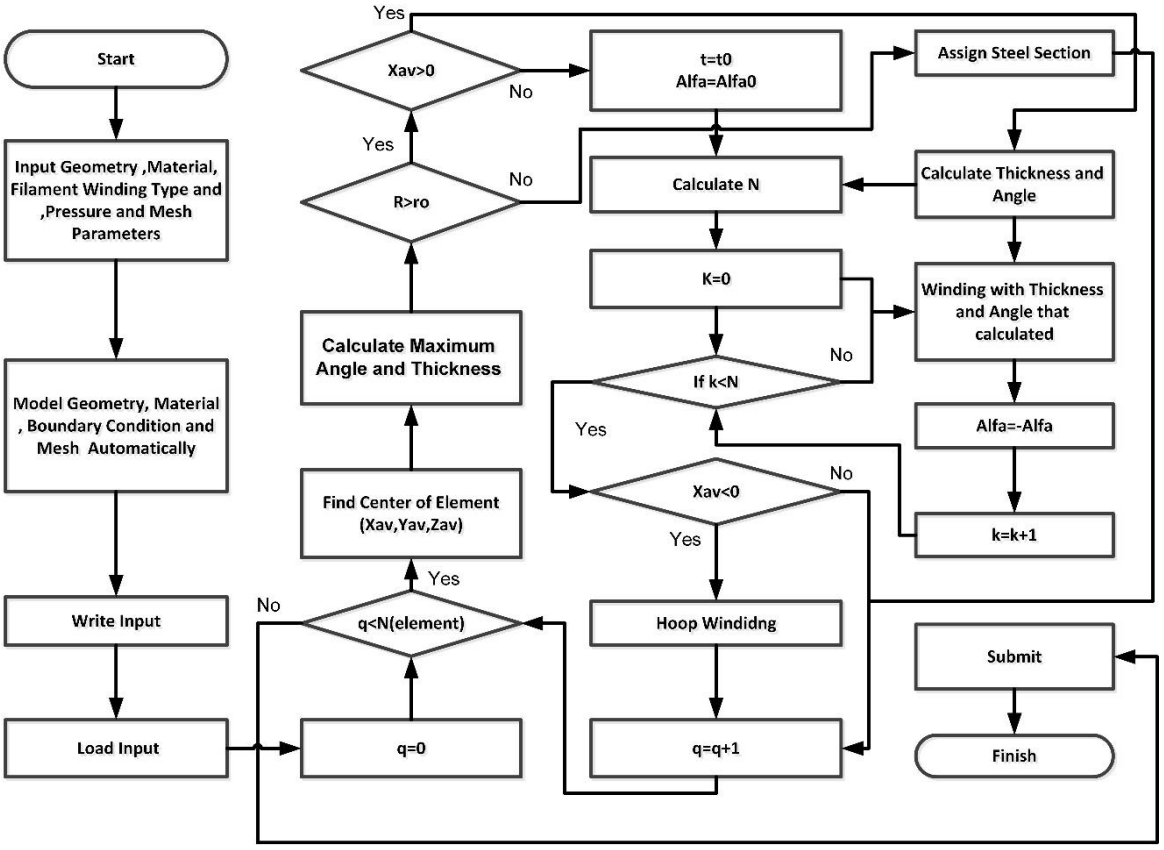

Fig. 7 Flowchart of composite pressure hull modeling using Python script

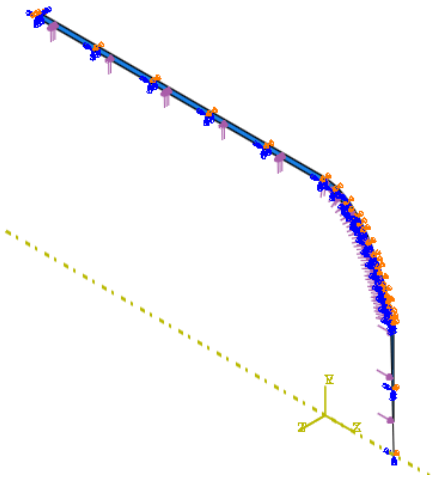

Fig. 8 The geometry model and boundary condition used in scripting method for simulation of composite pressure hull

Since ellipse mandrels are used widely, in this study filament wound geometry is assumed as an ellipse with 2a vertical diameter and horizontal diameter of 2b.

4.1 Material properties and layup

The implemented T700/epoxy elastic material properties and Tsai-Hill failure criterion parameters are shown in Table 2. As it can be seen, winding thicknesses in cylinder is 50mm for helical winding and 20 mm for hoop winding. Moreover, the thickness of one helical layer is 0.5mm.

By changing a/b ratio and the winding angle in two approaches used for winding within a certain range, an optimum model (which considers both failure criterion and buckling) based with the maximum safety factor is obtained. In these models, the total length was assumed to be constant. Therefore, any variation in winding angle and a/b ratio may lead to different cylinder lengths of composite pressure hull.

Table 2 Material properties of T700

$E_1(Gpa)$	133	$X_T(MPa)$	2507
$E_2(Gpa)$	9.1	$X_C(MPa)$	1201
Nu_{12}	0.31	$Y_T(MPa)$	61.8
$G_{12}(Gpa)$	5.67	$Y_C(MPa)$	186
$G_{13}(Gpa)$	5.67	$S_{12}(MPa)$	84.8
$G_{23}(Gpa)$	3.5		

4.2 Optimization results in planar winding method

In Fig. 9, results obtained from different simulations performed using planar winding method are represented. Using these simulations the dependence of safety factor obtained based on the Tsai-Hill failure criterion and buckling pressureon winding angle and a/b ratio were studied. In order to study the influences of winding angle and a/b ratio more precisely, one of these two parameters was kept constant and the variations in safety factor against the other one was investigated periodically (see Fig. 9).

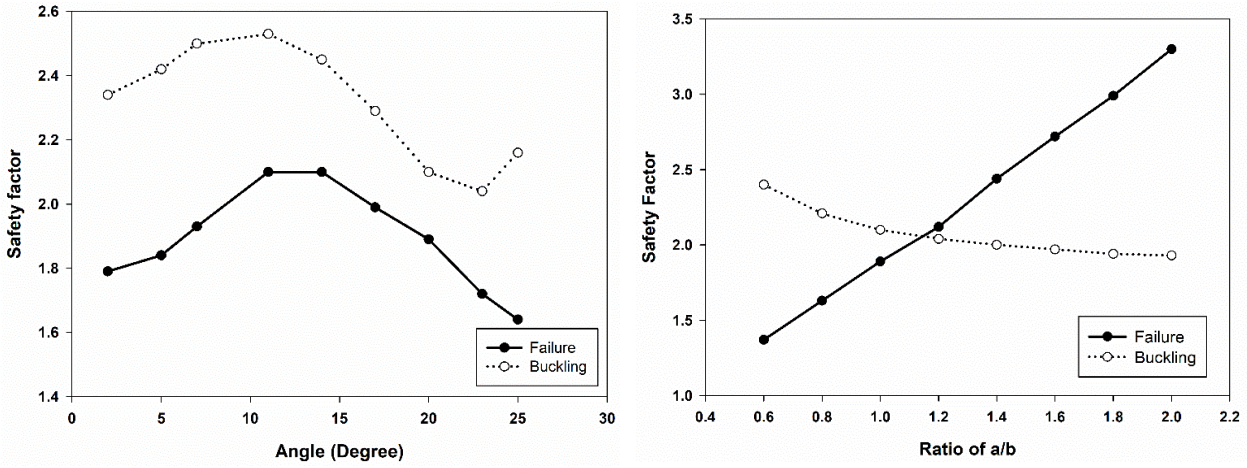

Fig. 9 Comparison of safety factor based on failure and buckling (a) winding angle with a/b=1 ratio vs (b) a/b ratiowith 20° winding angle for planar winding in composite pressure hull.

Results obtained from these simulations showed that the optimum winding angle and a/b ratio in planar winding are 11 and 1.2º, respectively. Two important results can be obtained from Fig. 9 (a). The first one is that the failure criterion is more critical than buckling and the second one is that neither of them shows a monotonic trend. From Fig. 9(b) one can conceive that failure criterion is more critical than buckling when a/b ratio is less than 1.2.

4.3 Optimization results in geodesic winding method

In this section, we first study the effect of winding angle on failure criterion and buckling pressure while keeping a/b constant. It is obvious from Fig. 10(a) that the winding angle is between 20° and 72° which is the angle of the opening adjacent band width. Afterwards, the effect of a/b ratio on failure criterion and buckling pressure for a winding angle of 20° are studied. The results obtained from this study are represented in Fig. 10(b)**Error! Reference source not found.**.

According to Fig. 10(a), neither the failure criterion nor buckling show a monotonic trend. In Fig. 10(b)**Error! Reference source not found.**, however, as the safety factor for bucking decreases, it increases for failure criterion. Finally, the results obtained from simulations show that for geodesic winding method, optimum winding angle and a/b ratio (i.e. the optimum safety factor) occurs at 45° and 1.2º, respectively.

It can be easily found from Figs. 9 and 10 that in both winding approaches, the safety factor shows the same trend. In both approaches, safety factor of buckling increases by increasing a/b ratio, while failure criterion decreases simultaneously. This phenomenon may be related to the increase of cylinder length.

Supposing a constant radius, increasing a/b ratio results in an increase in cylinder length, which in turn reduces buckling safety factor.

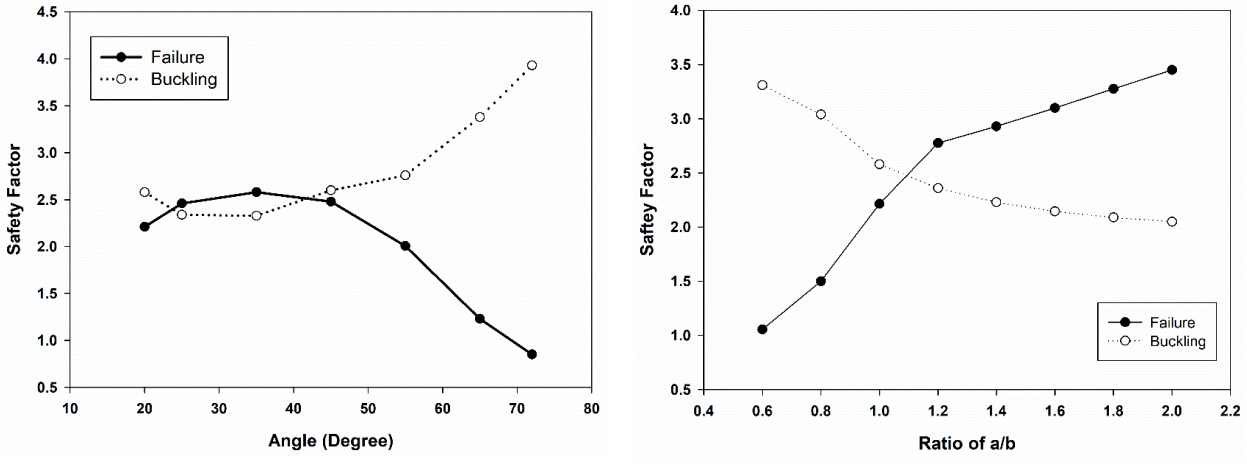

Fig. 10 Comparison of safety factor based on failure and buckling (a) winding angle with a/b=1 ratio vs (b) a/b ratio with 20^0 winding angle in geodesic winding for composite pressure hull

On the other hand, by increasing the a/b ratio, the length of ellipse part of composite pressure hull decreases. Therefore, the stressapplied on the interface between cylinder and dome is reduced as a result of the reduction of moment. These will result in an increase of failure criterion safety factor, since the interface between cylinder and dome is related to the maximum failure criterion.

According to the results obtained for the composite pressure hull, a composite pressure hull with a winding angle of 45° and a a/b ratio of 1.2 was simulated separately and it was shown that this model the maximum safety factor, confirming that the optimum model has been selected correctly.

5. Puck failure implementation

UMAT subroutine based on Puck failure criterion equations (see Table.1) was used in ABAQUS software. The flowchart of UMAT subroutine is shown in Fig. 11. The validation of the subroutine was performed first, afterwards the optimum model obtained in the previous section was analyzed by considering material degradation. Such a program can distinguish between different modes of failure. The validation of the program was performed by constructing a comparison between the curves of puck failure criterion in ref [36] for several types of loading and different material properties as follows:

Stage1: Combination of loading perpendicular to the fiber direction and shear loading

Stage2: Combination of fiber direction loading and shear loading

Stage3: Combination of fiber direction loading and perpendicular to the fiber direction loading

Fig. 12, 13, and 14 represents the results of simulation conducted using UMAT subroutine and compare them with Puck failure curve for these three loading stages [36], respectively.

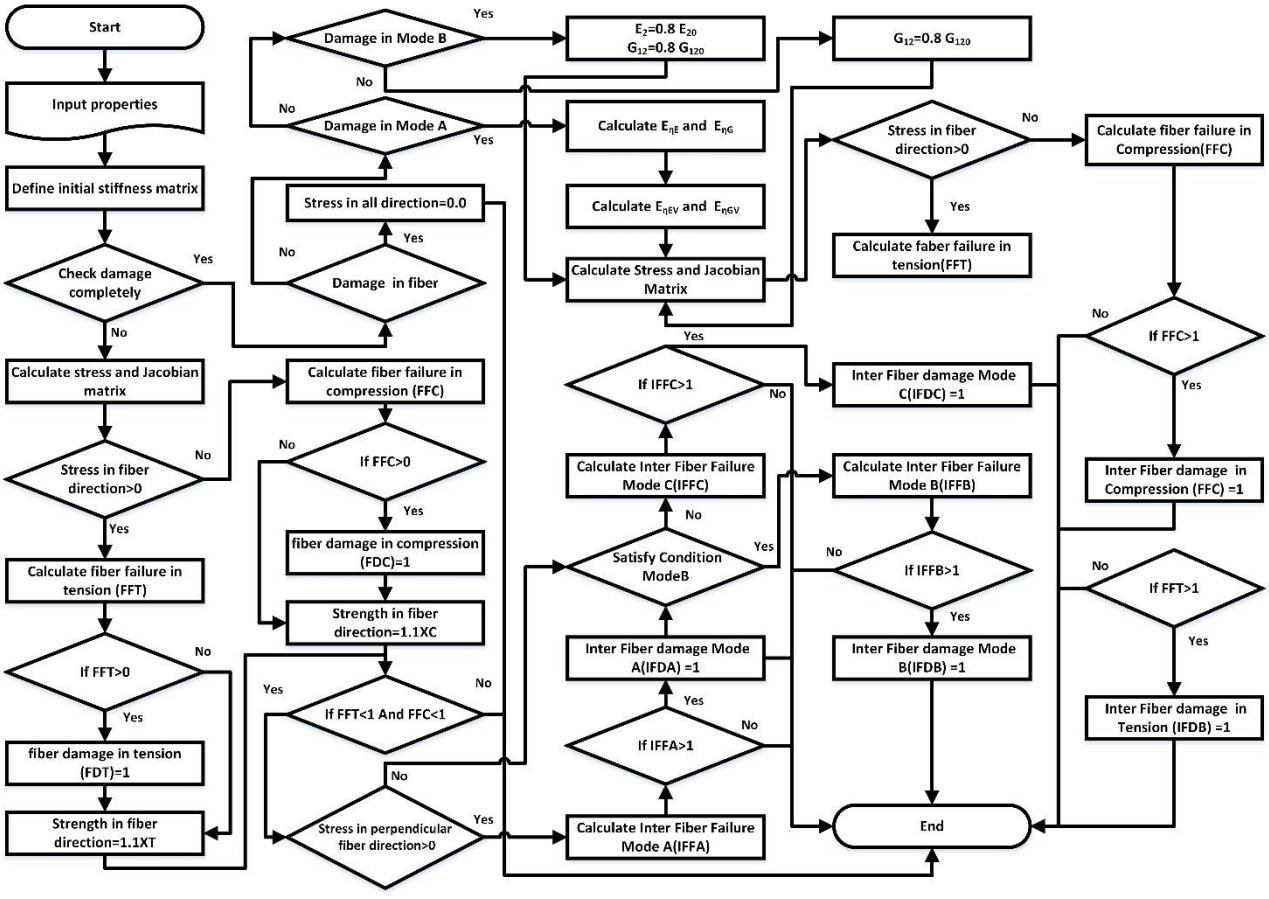

Fig. 11 UMAT subroutine flowchart for Puck progressive failure

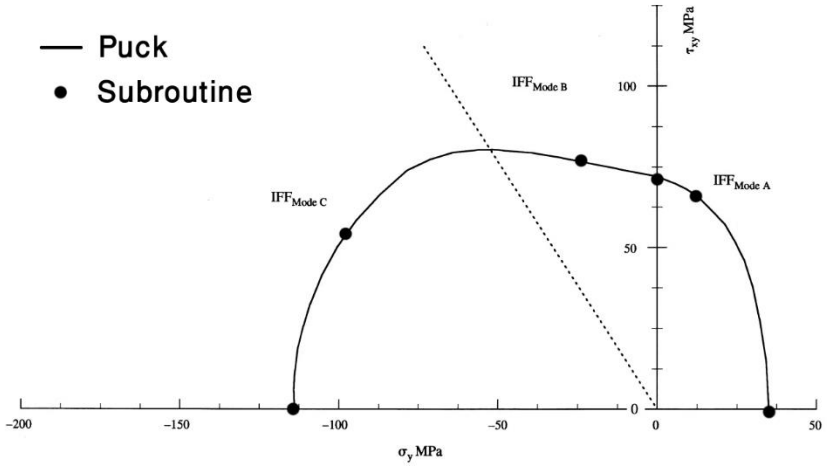

Fig. 12 Comparison between UMAT subroutine results and ref [33] to identify failure initiation in combination of perpendicular to the fibers direction loading and shear loading of E-glass (21xK43Gevtex)/LY556 composite

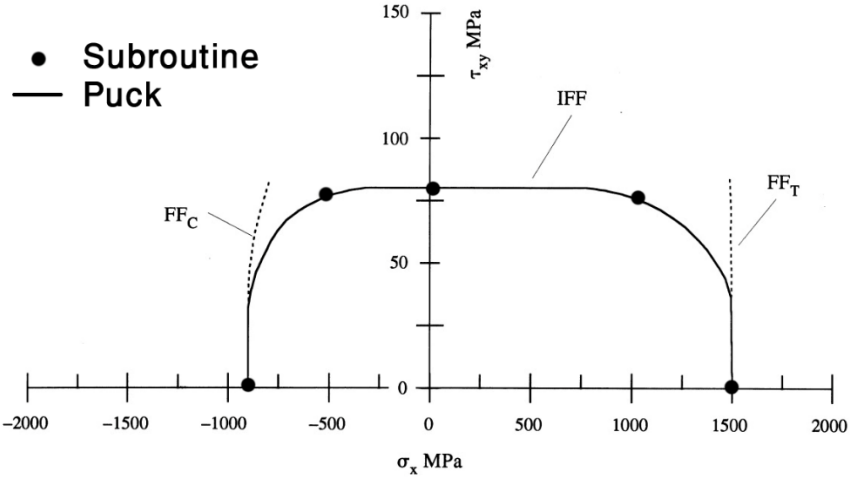

Fig. 13 Comparison between UMAT subroutine results and ref [33] to identify failure initiation in combination of fibers direction loading and shear loading of T300/BSL914C composite

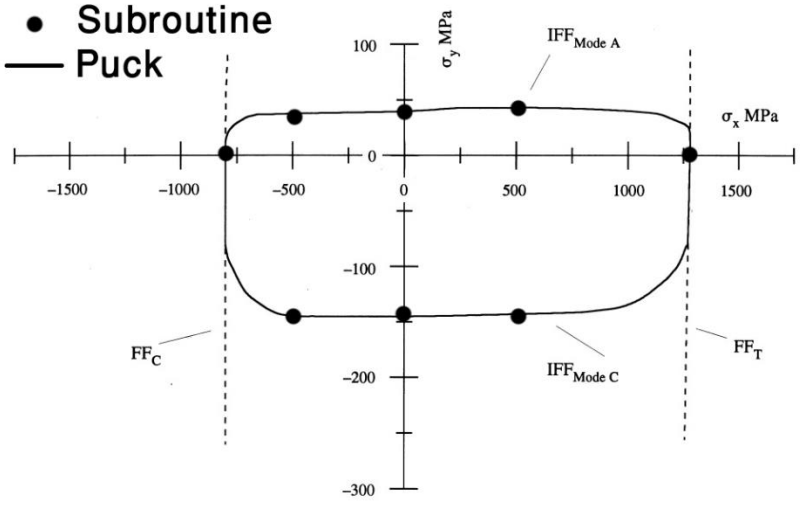

Fig. 14 Comparison between UMAT subroutine results and ref [33] to identify failure initiation in combination of fiber direction loading and perpendicular to the fiber direction loading of E-Glass/MY750 composite

As it can be seen from Figs. 11-14, there is a good agreement between UMAT subroutine results and results presented in ref [36].

6. Application of Puck failure for optimum composite pressure hull

Optimum composite pressure hull was simulated in ABAQUS software. During such a simulation, composite pressure hull was modeled thoroughly. Geometric properties of the optimum composite pressure hull is shown in Table 3. In addition, shell element (S4R) was used and one point of model was fully constrained to restrain rigid motion. Loading was performed in two steps. In the first step, loading was performed to identify failure initiation and in the second, load increased to the fiber failure. It is worth noting that during the second step, the applied load was increased gradually to guarantee the precise modeling of the progressive failure. Puck failure criterion was to determine the initiation and propagation of failure. In this configuration, failure initiates at 28.6 MPa, however, the hull withstands up to 50.6MPa. As the pressure exceeds 50.6 MPa, failure occurs.

Table 3 Geometry properties and winding angle of optimum composite pressure hull model

Winding Angle	45 degree
$\frac{a}{b}$ **ratio**	1.2
Diameter	2200mm
Length	1100mm
Helical Winding	50mm
Hoop winding	20mm

Fig. 15 indicates that the distribution of stress in the cylinder region, where hoop layer is wounded on helical layers, is uniform. In addition, as can be seen in Fig. 15 and Fig**. 16**, failure initiates in bottom layer near the interface between cylinder and dome in mode C (28.6MPa). Bending in this region due to the non-uniformity in thickness and high stress concentration leads to this failure.

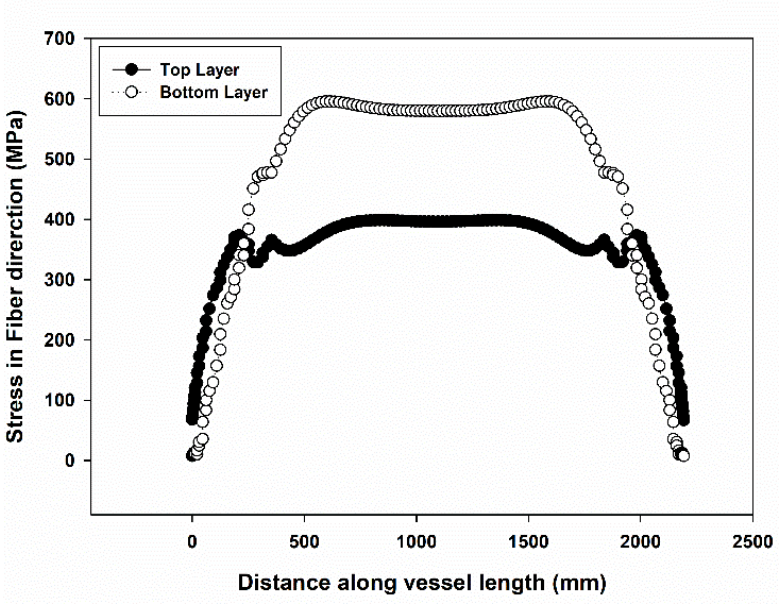

Fig. 15 Stress in fiber direction for bottom and top layers of composite laminate in composite pressure vessel

Failure mode C is an indication of matrix weakness. Therefore, the pressure at which damage initiates may be increased in the case of a stronger matrix. When the pressure increases to 37.4 MPa, mode A of Puck failure in the opening of pressure hull is activated (see Fig. 17). This failure happens due to the bending in the interface between plug and composite pressure hull. When the stress reaches 40.3MPa, failure of fiber under compression occurs. This failure leads to buckling and fiber failure under tension consequently (see Fig. 17). The reason of this kind of failure is weakness in some region due to fiber failure.

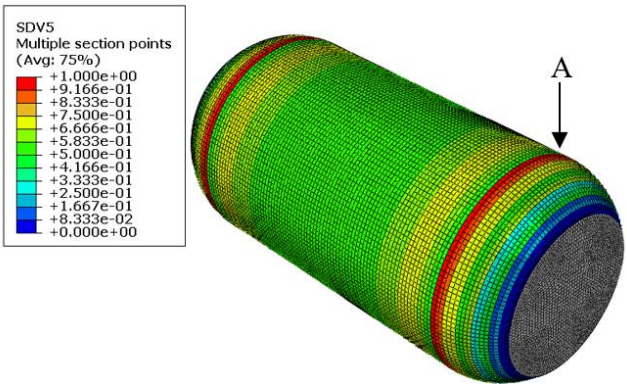

Fig. 16 Mode C failure initiation contour in optimum pressure hull with E-glass (21xK43Gevtex)/LY556 composite material

Linear buckling analysis was performed. According to Fig. 18.a., the shape of the first mode is the same as the final shape of progressive puck failure criterion analysis (see Fig. 18.b). From this observation, one can conclude that progressive failure causes buckling.

Moreover, the risk analysis of composite pressure hull was performed. In Table 4 , buckling pressures for three approaches of simulation are reported. As can be seen, the pressure buckling of progressive failure analysis and the risk analysis have the same value, both of which are less than linear buckling. This seems reasonable, since buckling is originally a nonlinear phenomenon. Radial displacement against pressure diagram in element A by considering types of failure is shown in Fig. 17 and is determined in Fig. 18.

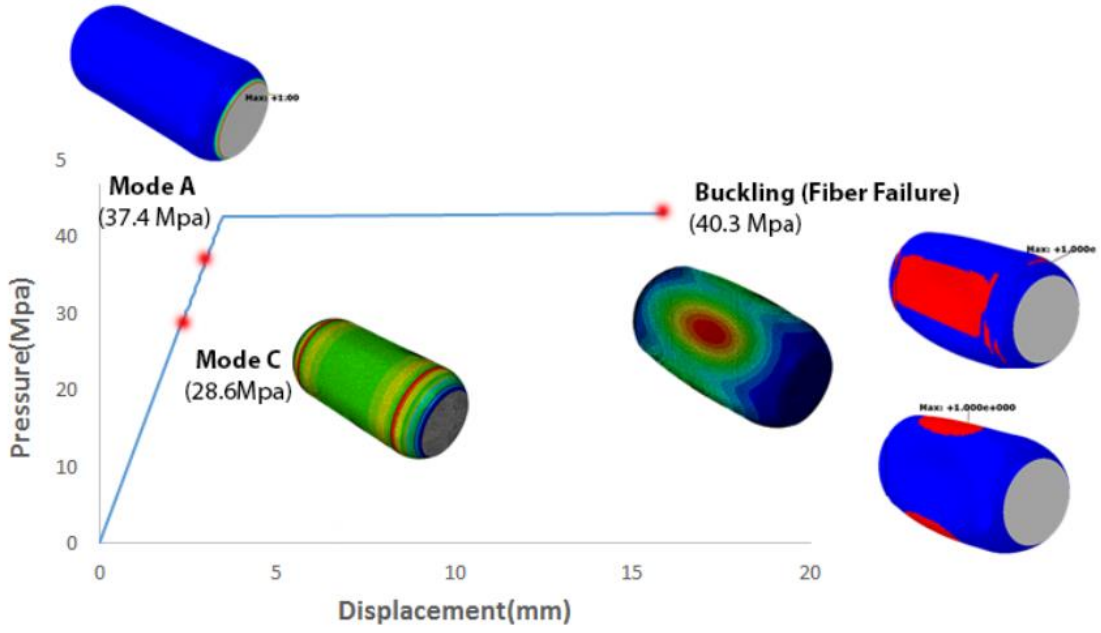

Fig. 17 Radial displacement vs. Pressure in element A (Fig. 16) by considering types of Puck failure in composite pressure hull

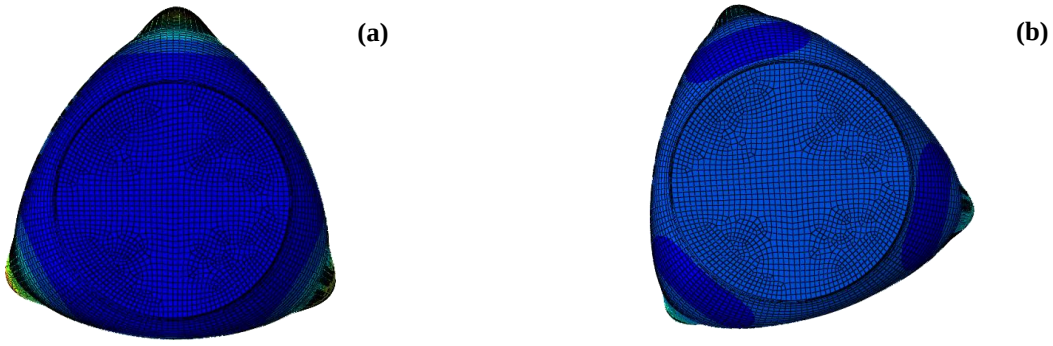

Fig. 18 (a) First mode shape of linear buckling analysis and (b) Final shape of progressive puck failure criterion analysis of composite pressure hull

Table 4 Buckling pressure for three methods of composite pressure hull simulation

Method	Progressive Failure analysis	Risk analysis	Linear buckling analysis
Buckling pressure(MPa)	43	43.8	44.61

7. Conclusion

In this paper, the strength and stability of an elliptical composite deep-submerged pressure hull was optimized. The optimization was performed considering two different filament winding patterns, i.e. geodesic and planar. The numerical modeling of the pressure hull under hydrostatic pressure was carried out in ABAQUSusing Python script and a damage model subroutine. Puck failure criterion was chosen for failure prediction. Two approaches, one based on partitions and the other based on scripting were introduced for the simulation . In the first method, sequence layup and thickness were calculated in MATLAB framework and assigned to each segment. In the second method, after meshing the model, position of each element were calculated and by considering geodesic winding or planar winding equation, thickness and sequence layup were assigned through scripting. The results indicate that the second method, in comparison with the first one, would be more reasonable choice because of more smoothness and less discontinuities of failure criterion. Angle and elliptic geometry optimization for planar and geodesic winding by python scripting method showed that geodesic winding with 45° winding angle and a/b=1.2 (feature of elliptic geometry) was the optimum composite pressure hull to withstand external pressure against failure and buckling. Tsai-Hill failure criterion were used to detect failure initiation in the composite pressure hull. In addition, the ultimate pressure for the composite pressure hull was determined. To this purpose, it is required that the failure initiation be detected precisely. Based on WWFE, Puck failure criterion was selected and a UMAT subroutine was written and verified with Puck curve (Ref [36]). Finally, the optimum composite pressure hull using the UMAT subroutine was simulated using the UMAT subroutine to detect progressive failure. It has been demonstrated that, the ultimate pressure was almost 1.5 times more than the pressure in failure initiation.

In addition, the following observations were obtained during the study:

1- Damage in composite pressure hull initiates in mode C. This indicates that failure occurs due to the weakness of matrix. Failure position is in the connection between the cylinder and dome. It happens due to discontinuity and stress concentration.
2- As the load increase, mode A failure in opening will appear. This failure can occur due to bending in the opening in the interface between plug and composite.
3- By further increasing the load, fiber failure under compression occurs and this follows by buckling. Afterwards, tensile fiber failure under bending occurs. This post-buckling phenomenon be described using both linear and nonlinear analyses.

8. Recommendations

For future studies, these works are suggested:

1- Using 3D continuum element to reduce error.
2- Implementation of angle variation within thickness due to changes in radius.
3- Using other materials like glass/epoxy and Kevlar/epoxy and comparing results with this simulation.
4- Using composite wound modeler commercial plug-in for ABAQUS for simulation of composite pressure hull and comparing the results with the scripting method presented in this study.

9. References

References

1. Pattison, "Design of Submarine Structures," Bristol 2001

2. Smith, C.S.: Design of Marine Structures in Composite Materials. Elsevier, London (1990)

3. Mouritz, A.P., Gellert, E., Burchill, P., Challis, K.: Review of advanced composite structures for naval ships and submarines. Compos. Struct. 53(1), 21–42 (2001)

4. Almeida Jr., J.H.S., Faria, H., Marques, A.T., Amico, S.C.: Load sharing ability of the liner in type III composite pressure vessels under internal pressure. J. Reinf. Plast. Compos. 33(24), 2274–2286 (2014)

5. Tafreshi, A.: Delamination buckling and postbuckling in composite cylindrical shells under combined axial compression and external pressure. Compos. Struct. 72(4), 401–418 (2006)

6. Mistry, J., Gibson, A.,Wu, Y.-S.: Failure of composite cylinders under combined external pressure and axial loading. Compos. Struct. 22(4), 193–200 (1992)

7. Gheshlaghi, R.M., Hojjati, M.H., Daniali, H.R.M.: Analysis of composite pressure vessels. In: Gdoutos, E.E. (ed.) Fracture of Nano and Engineering Materials and Structures: Proceedings of the 16th European Conference of Fracture, Alexandroupolis, Greece, July 3–7, 2006, pp. 335–336. Springer Netherlands, Dordrecht (2006)

8. Błachut, J.: Buckling of externally pressurized shallow spherical caps from composites. Mech. Adv. Mater. Struct. 18(2), 96–105 (2011)

9. Mian, H.H., Wang, G., Dar, U.A., Zhang, W.: Optimization of composite material system and lay-up to achieve minimum weight pressure vessel. Appl. Compos. Mater. 20(5), 873–889 (2013)

10. Walker, M., Smith, R.E.: A technique for the multiobjective optimisation of laminated composite structures using genetic algorithms and finite element analysis. Compos. Struct. 62(1), 123–128 (2003)

11. Rao Yarrapragada, K., Krishna Mohan, R., Kiran, B.V.: Composite pressure vessels. International Journal of Research in Engineering and Technology. 1(4), 597–618 (2012)

12. Pelletier, J.L., Vel, S.S.: Multi-objective optimization of fiber reinforced composite laminates for strength, stiffness and minimal mass. Comput. Struct. 84(29), 2065–2080 (2006)

13. Gomes, H.M., Awruch, A.M., Lopes, P.A.M.: Reliability based optimization of laminated composite structures using genetic algorithms and artificial neural networks. Struct. Saf. 33(3), 186–195 (2011)

14. Marín, L., Trias, D., Badalló, P., Rus, G., Mayugo, J.: Optimization of composite stiffened panels under mechanical and hygrothermal loads using neural networks and genetic algorithms. Compos. Struct. 94(11), 3321–3326 (2012)

15. Topal, U., Uzman, Ü.: Multiobjective optimization of angle-ply laminated plates for maximum buckling load. Finite Elem. Anal. Des. 46(3), 273–279 (2010)

16. Lee, G.-C., Kweon, J.-H., Choi, J.-H.: Optimization of composite sandwich cylinders for underwater vehicle application. Compos. Struct. 96, 691–697 (2013)

17. Bakshi, K., Chakravorty, D.: First ply failure study of thin composite conoidal shells subjected to uniformly distributed load. Thin-Walled Struct. 76, 1–7 (2014)

18. Liang, C.-C., Chen, H.-W., Jen, C.-Y.: Optimum design of filament-wound multilayer-sandwich submersible pressure hulls. Ocean Eng. 30(15), 1941–1967 (2003)

19. Zu, L., Koussios, S., Beukers, A.: Shape optimization of filament wound articulated pressure vessels based on non-geodesic trajectories. Compos. Struct. 92(2), 339–346 (2010)

20. Messager, T., Pyrz, M., Gineste, B., Chauchot, P.: Optimal laminations of thin underwater composite cylindrical vessels. Compos. Struct. 58(4), 529–537 (2002)

21. Maalawi, K.: Optimal buckling design of anisotropic rings/long cylinders under external pressure. J. Mech. Mater. Struct. 3(4), 775–793 (2008)

22. Almeida Jr., J.H.S., Ribeiro, M.L., Tita, V., Amico, S.C.: Damage and failure in carbon/epoxy filament wound composite tubes under external pressure: experimental and numerical approaches. Mater. Des. 96, 431–438 (2016)

23. Almeida Jr., J.H.S., Ribeiro, M.L., Tita, V., Amico, S.C.: Damage modeling for carbon fiber/epoxy filament wound composite tubes under radial compression. Compos. Struct. 160, 204–210 (2017)

24. Park, J.-S., Hong, C.-S., Kim, C.-G., Kim, C.-U.: Analysis of filament wound composite structures considering the change of winding angles through the thickness direction. Compos. Struct. 55(1), 63–71 (2002)

25. Liang, C.-C., Chen, H.-W., Wang, C.-H.: Optimum design of dome contour for filament-wound composite pressure vessels based on a shape factor. Compos. Struct. 58(4), 469–482 (2002)

26. W. E. Howard, "Design and Analysis Tools for Filament-Wound Composite Pressure Vessels with Elliptical Domes," 2001

27. Soden, P., Kaddour, A., Hinton, M.: Recommendations for designers and researchers resulting from the world-wide failure exercise. Compos. Sci. Technol. 64(3), 589–604 (2004)

28. Puck, A., Schürmann, H.: Failure analysis of FRP laminates by means of physically based phenomenological models. Compos. Sci. Technol. 58(7), 1045–1067 (1998)